Title: Smelting condition identification for a fused magnesium furnace based on an acoustic signal

Author names and affiliations:

You Fu[a], Ninghui Wang[a,*], Zhen Wang[b], Zhiqiang Wang[a], Bing Ji[c], Xiaochen Wang[d]

[a]School of Electrical Engineering, Dalian University of Technology, Dalian 116024, China
[b]School of Innovation and Entrepreneurship, Dalian University of Technology, Dalian 116024, China
[c]Department of Engineering, University of Leicester, University Road, Leicester, LE1 7RH, UK
[d]Environmental Engineering Assessment Center of Liaoning Province, Shenyang, 110032, China

***E-mail address*:** ninghuiw@263.net (N. Wang), benjamin85100@126.com (Y. Fu), ueyou@sina.com (Z. Wang), wangzq@dlut.edu.cn (Z. Wang), bing.ji@leicester.ac.uk (B. Ji), wangxiao@163.com (X. Wang).

Corresponding author: Prof. Ninghui Wang

Address: Institute of electrostatics & special power supply, Dalian University of Technology, No. 2 Linggong Road, Gangjingzi District, Dalian, China.
Postal code: 116024
***E-mail address*:** ninghuiw@263.net
Tel.: +86 0411 84708576; **Fax:** +86 0411 84708576.

Smelting condition identification for a fused magnesium furnace based on an acoustic signal

Abstract

To promote energy efficiency during fused magnesium furnace smelting, four smelting states were introduced in the smelting stage: an unmelted state, semi–molten state, molten state, and overheating state. A smelting identification system to distinguish these smelting states was developed through the use of linear predictive coding and a principal component analysis algorithm. A new smelting condition identification system was obtained. Corresponding pilot productions were conducted to compare the differences between employing the method and not employing the method. All of the pilot production data showed that feeding raw materials over time during the overheating state and decreasing current injection in the molten state could reduce energy consumption as well as increase crystal purity.

Keywords:

Acoustic signal; Fused magnesium furnace; Linear predictive coding; Principal component analysis.

1. Introduction

Fused magnesia is an essential material that has been widely used in many industries, such as the chemical industry, metallurgical industry, electric apparatus industry, and aerospace industry. High-purity fused magnesia is mainly produced by the unique three phase ac fused magnesium furnace (FMF). **Fig. 1** shows a schematic diagram of FMF. It is well known that FMF smelts ore at a high temperature produced by arcs. However, loud noises are often produced, which are caused by the strong vibration of arcs inside the FMF. Moreover, the acoustic signal from these arcs contains a wealth of information regarding the FMF smelting condition. If analyzed properly, the acoustic signal can be used as a significant parameter to construct the next generation FMF intelligent control system. **Drouet and Nadeau (1982)** investigated the power of the arcs and time integral of the acoustic signal using an oscilloscope and demonstrated their remarkable correspondence**. Lv et al. (2013)** investigated the correlation between the arc sound signal and arc length by analyzing the characteristics of the arc sound during the welding process. **Fu et al. (2015)** found that the arc noise intensity of each characteristic frequency shows different distributions in different operation states of the FMF. **Matschullat *et al.* (2012)** proposed a sound-based control methodology for smelting and foaming slag. In recent years, the linear predictive coding (LPC) method and principal component analysis (PCA) have been widely used for acoustic signal recognition. **Mohammed *et al.* (2012)** used the LPC method in the identification of spoken language. **Xie *et al.* (2012)** applied PCA to reconstruct the power spectra of acoustic signals.

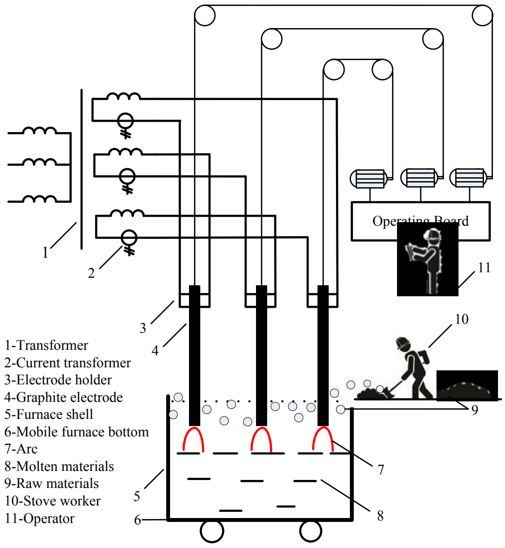

Fig. 1. Schematic diagram of a fused magnesia furnace.

In general, the smelting process of FMF can be divided into 3 stages: the starting stage, smelting stage, and ending stage. The smelting stage consumes more than ninety percent of the total electric energy in the FMF smelting process. Obviously, it is the most significant stage in throughout FMF smelting. In this stage, raw materials are dumped into the FMF every ten to fifteen minutes by stove workers. The raw material feeding moment has an enormous influence on the production efficiency. The materials cannot be melted completely if the raw materials are added into the FMF too early. Conversely, the materials would be overheated and high temperature melts would spurt out of the furnace if raw materials were added to the FMF too late. During the last decade, numerous FMF control systems have been created by Northeastern University, China. **Wu et al. (2008)** proposed an intelligent optimal control strategy using case-based reasoning for fused magnesia production. **Wu et al. (2009)** proposed a control method for the FMF smelting process based on rules acquired from operational experience. **Wu et al. (2011)** applied a neural network controller in a magnesium plant to reduce energy consumption. **Wu et al. (2012)** developed an intelligent operation control system by combing rule-based reasoning and switching control methodology. **Wu et al. (2015)** presented a data-driven identification and self-healing control system to address the abnormal conditions of the FMF smelting process. Three-phase voltages and currents are the main parameters of the FMF control system. Arcs are submerged under materials during the FMF smelting stage. The arc current and arc voltage cannot be measured directly. The complicated interactions between the arcs and materials cannot be described by the three phase voltages and currents. The main function of the FMF control system during the smelting stage is to passively adjust the height of the three electrodes to maintain the balance of the three phase currents. The smelting conditions of the materials cannot be identified automatically. Stove workers must determine when to feed raw materials into the furnace according to their experience. The smelting stage usually lasts eight to nine hours, and the stove workers must feed tons of raw materials every ten to fifteen minutes. Consequently, manual feeding brings a number of uncertain factors into the production of fused magnesia. A smelting condition identification system must be developed for the fused magnesia production line to realize automatic feeding of FMF.

In this investigation, an FMF smelting condition identification method based on the acoustical signal of arcs was proposed to improve the production efficiency of fused magnesia. A significant characteristic of this method was that a sound track model of arcs was introduced to distinguish different smelting conditions during the FMF smelting stage. First, some vectors, which represent different smelting conditions, were extracted from the arc sound using linear predictive coding (LPC). Next, through PCA, the dimensions of these vectors were reduced. Subsequently, a status map of the arc sound signal was constructed to distinguish different FMF smelting conditions. Thus, an online FMF smelting condition identification system based on both LabVIEW and Matlab was developed. The proposed FMF smelting condition identification system can replace stove workers to determine when to feed raw materials into FMF during the smelting stage. Pilot production proved that arranging the feeding time properly with the proposed smelting condition identification method can both reduce the energy consumption per ton and promote the purity of MgO crystals.

2. Sound track model of arcs

The evidence from high-speed photographic studies proved that arcs exist between the graphite electrodes and molten materials during the smelting stage **(Reynolds, 2011)**. The axial temperature produced by the arcs in the EAF is typically over 10 000 °C, thus causing the air around the arcs to ionize at high temperature **(Zweben, 2002)**. Molecules are ionized into positive ions and electrons. Through the electric field, positive ions converge into ion flow, whereas the electrons converge into electron flow. The arc is a type of plasma composed of neutral particles, positive ions, and electrons. The flow of plasma induces vibration of the surrounding medium. Thus, the vibration propagates in the form of sound waves both in and out of the FMF. As a result, it is envisaged that the whole FMF could be equivalent to a resonant cavity. The reciprocity between the arcs and the raw materials changes the arc length. Meanwhile, the characteristics of the arc track in the FMF change under different smelting conditions. Different smelting conditions of the FMF can be distinguished according to the characteristics of the arc sound track. **Bi et al. (2011)** considered the arc sound track as a distributed system and adopted an auto regression model to estimate the arc sound track:

$$H(z) = \frac{s(z)}{u(z)} = \frac{G}{1 - \sum_{k=1}^{P} a_k z^{-k}} \tag{1}$$

where $H(z)$ is the transfer function of a certain smelting condition, $s(z)$ is the Z transformation of $s(n)$, $s(n)$ is the acoustic output signal sequence of FMF arc sound, $u(z)$ is the Z transformation of $u(n)$, $u(n)$ is the excitation source of $s(n)$, G is the gain factor, p is the order number of the full pole model, and a_k is the parameter of the model; each smelting condition corresponds to a certain set of parameters. If the order number of the model p and parameter a_k of each smelting conditions are known, then the computer can distinguish between different FMF smelting conditions instead of stove workers.

3. FMF sound track parameters estimation

The parameters of the FMF sound track model were estimated using the LPC method. The calculation progress of LPC can be summarized in the following steps.

First, the difference equation between $s(n)$ and $u(n)$ is induced according to equation (1):

$$s(n)=\sum_{k=1}^{p}a_k s(n-k)+Gu(n) \tag{2}$$

Second, a predictor is defined as follows:

$$\hat{s}(n)=\sum_{k=1}^{p}a_k s(n-k) \tag{3}$$

Third, the forecast error is calculated using the following formula:

$$e(n)=s(n)-\hat{s}(n)=s(n)-\sum_{k=1}^{p}a_k s(n-k) \tag{4}$$

To ensure the channel model describes the arc sound as precisely as possible, the mean square error of the forecast error should reach its minimum. Thus, the energy of the average forecast error is defined by the following formula:

$$E=\sum_n e^2(n)=\sum_n[s(n)-\hat{s}(n)]^2=\sum_n[s(n)-\sum_{k=1}^{p}a_k s(n-k)]^2 \tag{5}$$

To ensure E reaches its minimum, each parameter a_k should satisfy the following equation:

$$\frac{\partial E}{\partial a_j}=2\sum_n s(n)s(n-j)-2\sum_{k=1}^{p}a_k\sum_n s(n-k)s(n-j)=0 \tag{6}$$

Next, a set of linear prediction equations was obtained:

$$\sum_{n} s(n)s(n-j) = \sum_{k=1}^{p} a_k \sum_{n} s(n-k)s(n-j) \qquad (1 \le j \le p) \tag{7}$$

Further, a new operator $\Phi(j, k)$ is constructed for the convenience of calculation:

$$\Phi(j,k) = \sum_{n} s(n-j)s(n-k) \tag{8}$$

The linear prediction equations (7) can be represented as follows:

$$\sum_{k=1}^{p} a_j \Phi(j,k) = \Phi(j,0) \qquad (1 \le j \le p) \tag{9}$$

Next, an autocorrelation function $r(j)$ is defined as:

$$r(j) = \sum_{n} s(n)s(n-j) \tag{10}$$

It can be proved that the relationship between $\Phi(j, k)$ and $r(j)$ is as follows:

$$\Phi(j,k) = \Phi(k,j) = r(|j-k|) \tag{11}$$

Thus, equation (9) can be represented as follows:

$$\begin{bmatrix} r(0) & r(1) & r(2) & \cdots & \text{-1)} \\ r(1) & r(0) & r(1) & \cdots & \cdot 2) \\ r(2) & r(1) & r(0) & \cdots & \cdot 3) \\ \vdots & \vdots & \vdots & \vdots & \vdots \\ r(p-1) & r(p-2) & r(p-3) & \cdots &) \end{bmatrix} \begin{bmatrix} a_1 \\ a_2 \\ a_3 \\ \vdots \\ a_p \end{bmatrix} = \begin{bmatrix} r(1) \\ r(2) \\ r(3) \\ \vdots \\ r(p) \end{bmatrix} \tag{12}$$

The matrix on the left side of the equation (12) is named the correlation function matrix. In addition, it can be observed that the symmetric axis of this matrix is its primary diagonal. All of the elements on the primary diagonal are equal. All of the elements on any oblique stroke that are parallel to the primary diagonal are equal. This type of matrix is called a Toeplitz matrix. Equation (12) is called the Yule-Walker equation. To avoid a large number of calculations, the Levinson-Durbin recursive algorithm was used to obtain the coefficients $a_1, a_2, \cdots, a_p$.

The acoustic signal of FMF changes with time. LPC analysis of the signal is a short-time analysis. Computers cannot process infinite amounts of signal. Hence, it is necessary to use a window function to extract a set of data from the original acoustic signal. The rectangular window often causes frequency leakage, whereas, the Hamming window has a high frequency resolution and good performance for the arc sound frequency and can reduce the frequency leakage. The signal was windowed before the coefficients were solved.

$$s_w(n) = s(n)w(n) \tag{13}$$

where $w(n)$ is a window function and $s_w(n)$ is the windowed signal of $s(n)$.

4. Experimental setup

The experimental setup of the FMF smelting condition identification system is shown in **Fig. 2**; the system included a microphone, tripod, SMB–BNC cable, dynamic signal acquisition module, lithium battery, Ethernet chassis, network cable, and industrial personal computer. The microphone was G.R.A.S. 40PH free field array microphone, which was fixed on a tripod with telescopic legs. The SMB–BNC cable connected the microphone and the dynamic signal acquisition module. The dynamic signal acquisition module that was used to perform the high accuracy audio frequency measurements was a NI 9234. The resolution of the module was 24 bits. The module was plugged into an Ethernet chassis (NI 9181). For the convenience of measurement in the smelting site, a 50 000 mAh lithium battery was used as the power supply of the

Ethernet chassis. A network cable was used to connect the Ethernet chassis and an industrial personal computer. Both FMF sound signal acquisition and sound track parameter estimation were realized with LabVIEW graphic coding. The industrial personal computer sent control instructions to the operating board of the FMF via a serial port.

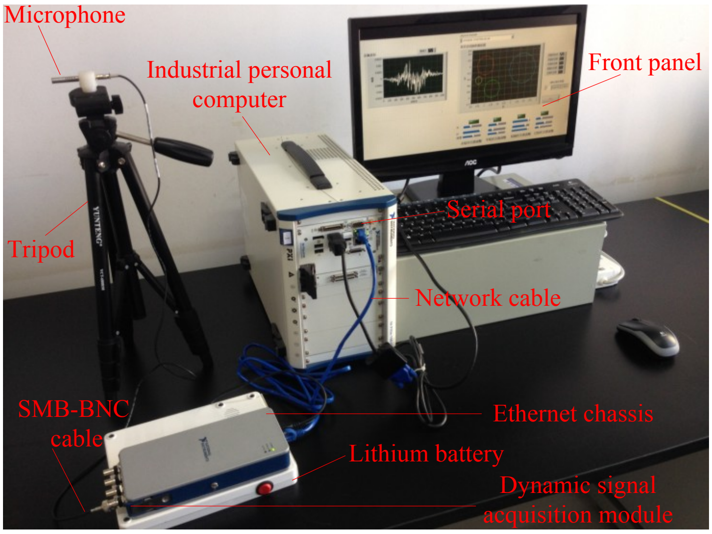

Fig. 2. Experimental setup for the FMF smelting condition identification system.

The position of the FMF sound measurement point is shown in **Fig. 3**. The microphone and tripod were placed at the measurement point. The telescopic legs of the tripod were adjusted to set the microphone 2 m above the furnace bottom. The FMF sound signal acquired at the measurement point in **Fig. 3** contains the sound emitted from both the furnace top and furnace shell. Moreover, the FMF sound signal at that point could not be masked by the noise from the transformer **(Haering et al, 1979)**. In the present work, the newly built FMF with the power of 5 000 kVA was taken as the research object. The detail dimension of the FMF is shown in **Table 1**.

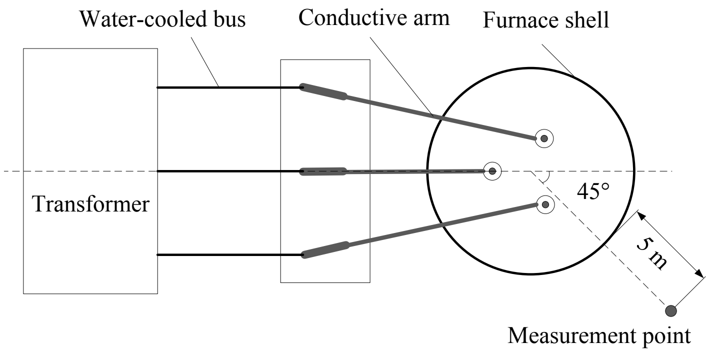

Fig. 3. The position of the FMF sound measurement point.

Table 1 Dimensions of the fused magnesium furnace.

Items	Dimension (mm)
Electrode diameter	350
Diatance between electrodes	880
Electrode operating depth	2 000
Furnace shell diameter	2 500
Furnace shell height	2 000

5. Experiments and analysis

5.1 LPC waveform reconstruction

According to the time–frequency characteristics of the FMF arc sound **(Fu et al., 2015)**, the pitch period of the FMF sound was identified to be 10 ms. In addition, the frame length was 24 ms, and the sample points of each frame was 1200. Next, a frame of FMF sound in the smelting stage was acquired. Afterwards, the acquired acoustic signal was multiplied by the Hamming window. Specifically, the Hamming window was implemented using a subroutine module in the LabVIEW Functions Tab. Next, the Levinson-Durbin recursive algorithm was adopted to obtain the coefficients a_1, a_2, ⋯, a_p. It is well known that higher a LPC order number leads to higher prediction accuracy. The calculation amount increases with the order number. In practical engineering application, a small order number can be used in the calculation as long as the mean forecast error meets the requirement. **Bi et al. (2011)** used a 10-order LPC model to estimate the arc sound track in metal inert gas welding and obtained satisfactory results. In this investigation, a 10-order LPC model was used to reconstruct the FMF sound signal. The LPC function in Matlab was used to calculate the LPC coefficients and to reconstruct the waveform. The LPC reconstructed waveform of a frame FMF sound signal during the smelting stage is illustrated in **Fig. 4**. One can observe that the reconstructed signal waveform was consistent with the windowed signal waveform. Moreover, the relative tolerance of the reconstructed signal was generally smaller than 5%. Ten-order LPC analysis is found to be a reasonable estimate for the FMF sound track.

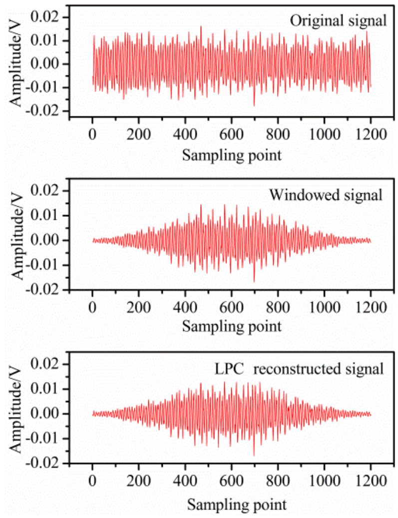

Fig. 4. LPC reconstructed waveform of the FMF sound

5.2 Feature vectors extract

Four-thousand frames of the acoustic signals under four different smelting conditions were acquired, and the feature vectors of each frame was obtained using the following steps:

(1) Record both the acoustic signal and smelting conditions in the FMF smelting stage of a smelting process.

(2) Extract 100 frames of the acoustic signal from each smelting condition, with each frame consisting of 1200 sample points.

(3) Filter each frame using the Hamming window.

(4) Calculate the LPC parameters using Matlab.

(5) Calculate the average LPC parameters value of each smelting condition.

(6) Repeat Step (1) to Step (5) 10 times and obtain 10 sets of LPC parameters for each smelting condition.

(7) Calculate the average LPC parameters value of each smelting condition in Step (6).

The average value of the 10-order LPC parameters of each smelting condition are listed in **Table 2**. The LPC parameters of the FMF sound track model were used to develop the smelting condition feature vector during the smelting stage, (a_1, a_2, ⋯, a_{10}).

Table 2 Average LPC parameters in diffenrent smelting states.

State	Unmelted	Semi–molten	Molten	Overheating
a_1	−1.057	−1.317	−1.355	−0.864
a_2	0.398	0.649	1.093	0.371
a_3	−0.391	−0.436	−0.826	−0.368
a_4	0.504	0.345	0.728	0.236
a_5	−0.263	−0.238	−0.366	−0.184
a_6	0.227	0.276	0.610	0.182
a_7	−0.035	0.050	−0.462	−0.049
a_8	0.195	−0.142	0.081	0.077
a_9	−0.218	0.086	−0.061	−0.073
a_{10}	0.071	−0.046	0.111	0.024

The following 10D smelting condition feature vectors were used to predict the unmelted state, semi–molten state, molten state, and overheating state:

$$A_1 = (-1.057, 0.398, -0.391, 0.504, -0.263, 0.227, -0.035, 0.195, -0.218, 0.071)^T \quad (14)$$

$$A_2 = (-1.317, 0.649, -0.436, 0.345, -0.238, 0.276, 0.050, -0.142, 0.086, -0.046)^T \quad (15)$$

$$A_3 = (-1.355, 1.093, -0.826, 0.728, -0.366, 0.610, -0.462, 0.081, -0.061, 0.111)^T \quad (16)$$

$$A_4 = (-0.864, 0.371, -0.368, 0.236, -0.184, 0.182, -0.049, 0.077, -0.073, 0.024)^T \quad (17)$$

These four smelting condition feature vectors can be used to distinguish the different smelting states. The 10D smelting condition vector is inconvenient to graphically illustrate. There may be a relationship between the parameters of a certain smelting state. To reduce the correlation and redundancy between the parameters, the dimensions of the smelting condition feature vectors should be reduced. Theoretically, the smelting condition feature vectors are dependent on the conditions of the arc sound track inside the furnace. Different process parameters, such as the arc current, arc voltage and raw material feeding moment, cannot change the sound track characteristics of the electric arc furnace. These 4 smelting condition feature vectors that are suitable for all of the fused magnesium furnace smelting processes, with different process parameters for the same furnace.

5.3 PCA dimension reduction

High-dimensional feature vectors are difficult to understand and impossible to display on the computer screen. On the contrary, low-dimensional vectors, such as one-dimensional vectors and two-dimensional vectors, can be easily displayed on the screen and improve the system operation speed. The PCA method can be used to reduce the vector dimensions. The fundamental principle of PCA is to map high-dimensional feature vectors to a low-dimensional space. Low-dimensional vectors can represent the smelting state instead of high-dimensional vectors. The advantages of PCA dimensional reduction are reduced system resources and faster processing of feature matching. The steps of PCA dimension reduction for the FMF sound signal are as follows:

(1) Construct the matrix of the four smelting condition feature vectors.

$$\mathbf{A} = \begin{bmatrix} \mathbf{A}_1 & \mathbf{A}_2 & \mathbf{A}_3 & \mathbf{A}_4 \end{bmatrix} = \begin{bmatrix} a_{11} & a_{12} & a_{13} & a_{14} \\ a_{21} & a_{22} & a_{23} & a_{24} \\ \vdots & \vdots & \vdots & \vdots \\ a_{p1} & a_{p2} & a_{p3} & a_{p4} \end{bmatrix} \tag{18}$$

where p is the dimension of the smelting condition feature vector, $p = 10$.

(2) Take each element in matrix **A** and subtract the mean value of all of the elements on its corresponding line. As a result, a new matrix is obtained:

$$\mathbf{A}^* = \begin{bmatrix} a_{11}^* & a_{12}^* & a_{13}^* & a_{14}^* \\ a_{21}^* & a_{22}^* & a_{23}^* & a_{24}^* \\ \vdots & \vdots & \vdots & \vdots \\ a_{p1}^* & a_{p2}^* & a_{p3}^* & a_{p4}^* \end{bmatrix} \tag{19}$$

$$a_{ij}^* = a_{ij} - \frac{1}{4}\sum_{k=1}^{4} a_{ik} \tag{20}$$

(3) Calculate the covariance matrix of $\mathbf{A}^*$:

$$\mathbf{C} = \frac{1}{p}\mathbf{A}^*(\mathbf{A}^*)^T \tag{21}$$

(4) Solve both the eigenvalues and eigenvectors of matrix **C** from the following equation:

$$|\lambda \mathbf{I} - \mathbf{C}| = \mathbf{0} \tag{22}$$

Sort these eigenvalues λ_i (i=1, 2, ⋯, p) from large to small, $\lambda_1 \geq \lambda_2 \geq \cdots \geq \lambda_p$.

(5) Calculate the accumulative contribution rate of each eigenvalue and determine the dimensions of the feature vector after dimension reduction.

$$\frac{\sum_{k=1}^{i} \lambda_k}{\sum_{k=1}^{p} \lambda_k} \tag{23}$$

The accumulative contribution rates of all of the eigenvalues are shown in **Table 3**. The accumulative contribution rate of the first two eigenvalues was obviously greater than 95%. The principal components corresponding to the first two eigenvalues could be used to distinguish different smelting states instead of the 10D smelting condition feature vectors.

Table 3 The accumulative contribution rate of each eigenvalue.

	Eigenvalue	Accumulative contribution rate (%)
λ_1	0.093	78.7
λ_2	0.020	95.8
λ_3	0.005	100
λ_4~λ_{10}	0	100

(6) Use the eigenvectors $\boldsymbol{t}_1$ and $\boldsymbol{t}_2$ to construct a transform matrix **T**. Here, $\boldsymbol{t}_1$and $\boldsymbol{t}_2$ correspond to the eigenvalues λ_1 and λ_2, respectively.

$$\mathbf{T} = \begin{bmatrix} \mathbf{t}_1 & \mathbf{t}_2 \end{bmatrix} = \begin{bmatrix} -0.331 & 0.452 \\ 0.592 & -0.201 \\ -0.382 & -0.085 \\ 0.339 & 0.281 \\ -0.130 & -0.057 \\ 0.348 & 0.046 \\ -0.368 & -0.344 \\ -0.012 & 0.543 \\ 0.039 & -0.451 \\ 0.067 & 0.219 \end{bmatrix} \tag{24}$$

(7) Map the matrix of the four smelting condition feature vectors **A** to a new 2D

space via the transform matrix **T**.

$$\mathbf{B} = \mathbf{AT} \tag{25}$$

B is a matrix with four rows and two columns. The elements on the same row are the principal components of a smelting state and correspond to a point in the 2D space. **Table 4** shows the principal components of the four different smelting states.

Table 4 The principal components of different smelting states.

State	b_1	b_2
Unmelted	1.026	−0.125
Semi-molten	1.214	−0.708
Molten	2.092	−0.253
Overheating	0.829	−0.252

5.4 Smelting state identification

Fig. 5 shows the positions of the four sets of principal components in rectangular coordinates. On this FMF smelting status map, Point 1 is the benchmark of the unmelted state, Point 2 is the benchmark of the semi–molten state, Point 3 is the benchmark of the molten state, and Point 4 is the benchmark of the overheating state. During both the unmelted state and overheating state, the drastic fluctuations of arcs cause the instability of the FMF sound. The sound track features of these two smelting states are very similar. Point 1 and Point 4 are found to be nearest to each other, whereas, in the molten state, the blazing arcs inside the FMF produce a large noise. The benchmark of the molten state is located far from the other three benchmarks.

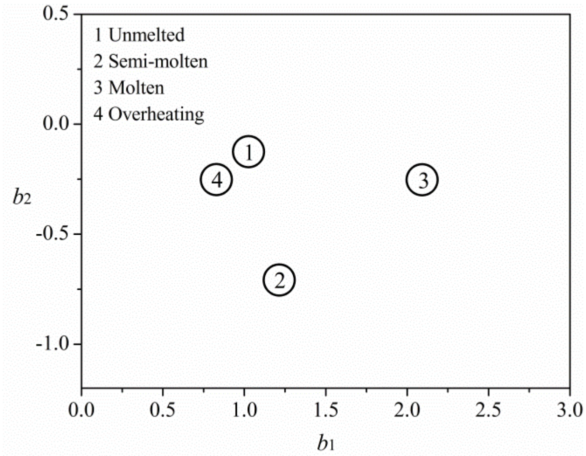

Fig. 5 FMF smelting status map.

The method to identify the smelting state with the FMF smelting status map can be described as follows:

(1) Capture a frame of the acoustic signal in the smelting stage.

(2) Filter the signal with a window function.

(3) Obtain a new set of 10-order FMF sound track parameters via the LPC method and construct a 10D column vector $\mathbf{A}_s$.

(4) Multiply $\mathbf{A}_s$ with the transform matrix $\mathbf{T}$ and obtain a new 2D row vector $\mathbf{B}_s$.

$$\mathbf{B}_s = \mathbf{A}_s \mathbf{T} \tag{26}$$

(5) Mark the location of $\mathbf{B}_s$ on the FMF smelting status map. The point on this location is the current state point.

(6) Calculate the distances from the current state point to Point 1, Point 2, Point 3, and Point 4.

(7) Determine the shortest distance in step (6), and the corresponding state of the point in the smelting status map is considered to be the FMF smelting state.

The recognition rate was quite low when the online recognition program was developed based on the method described above. The following situations usually occurred. The current state point was close to the unmelted benchmark, whereas the FMF was in the molten state. The current state point was close to the overheating benchmark, whereas the FMF was in the semi–molten state. It can be proposed that the distribution areas of different smelting states were different in the FMF smelting status map. The smelting states could not be distinguished accurately only according to the distances from the current state point to the smelting state benchmark point. Step (6) and Step (7) must be improved. Four smelting state circles were defined around each smelting state benchmark point. First, the smelting state of each point obtained in Step (5) was judged manually by the stove workers at the beginning of the FMF smelting stage. In addition, the radius of each circle was determined by the distribution of the corresponding state points. Moreover, the position of the center of each circle was adjusted according to the distribution of the state points. **Fig. 6** shows the LabVIEW block diagram of the FMF smelting condition identification program. **Fig. 7** shows the LabVIEW front panel of the FMF smelting condition identification program. This program displayed the data acquisition channel number of the microphone, waveform of a recent windowed FMF acoustic signal frame, and movements of the smelting state point. At the bottom of the front panel, some slide controls can be used to adjust the smelting state circles online. All of the state points on the FMF status map were exported to DIAdem for statistics after the smelting stage.

DIAdem is an interactive software for data management, data analysis, and generating reports. The distribution of state points on the smelting status map is shown in **Fig. 8**. Meanwhile, **Fig. 9** demonstrates the statistical analysis of the smelting states duration time.

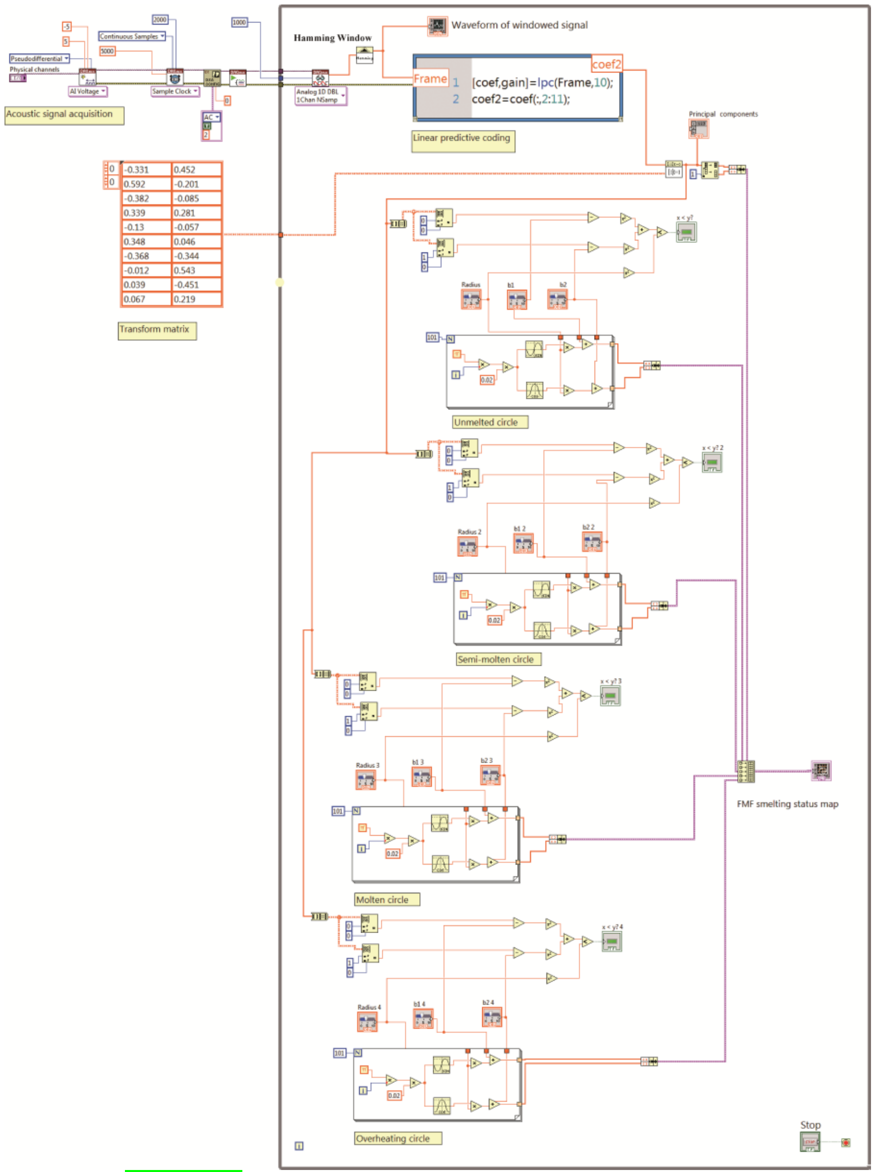

Fig. 6 LabVIEW block diagram of the FMF smelting condition identification

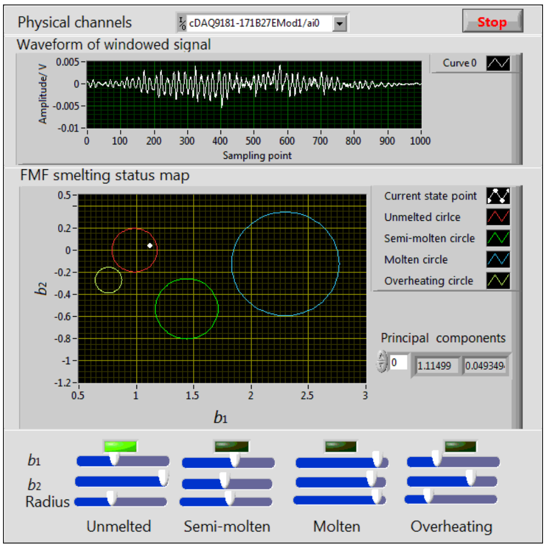

Fig. 7 LabVIEW front panel of the FMF smelting condition identification program.

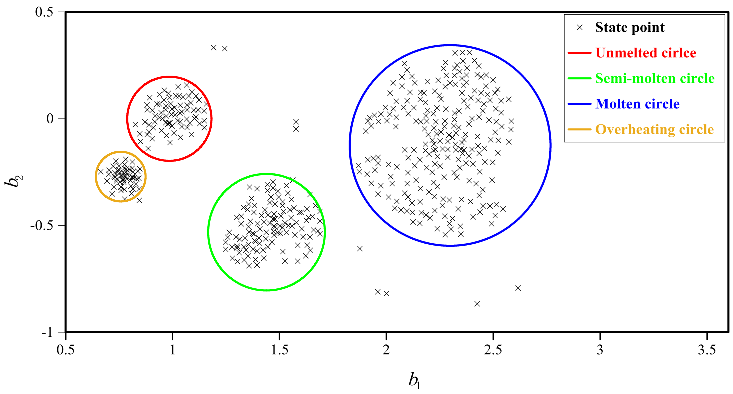

Fig. 8 Distribution of the state points on the smelting status map.

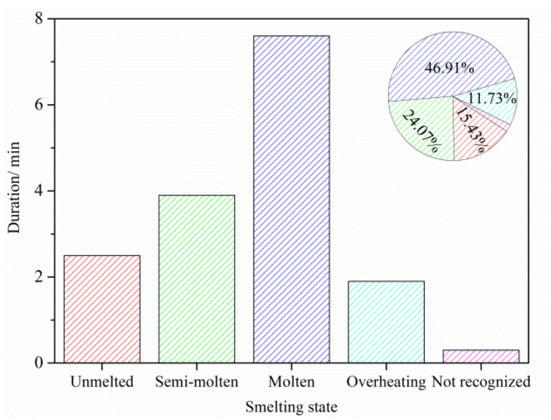

Fig. 9 Duration comparison of the four different FMF smelting states.

6 Industrial pilot production

6.1 Material feeding on energy consumption

The relationship of the raw material feeding moment and energy consumption per ton in fused magnesia production via FMF has confused many technicians. In the overheating state, the raw materials were completely melted. Meanwhile, large quantities of heat were wasted without more crystal production. The existing process in **Fig. 9** had a long overheating period. Thus, the overheating period in the smelting stage should be shortened. An effective solution is to adjust the raw material feeding time. Feeding raw material in the overheating state could force the FMF to enter the unmelted state. To prove the effectiveness of the process adjustment strategy above, stove workers were arranged to feed raw material into the FMF as soon as the program shown in **Fig. 7** demonstrated that the FMF entered the overheating state. The feeding amount at each time was 1.2 t, which was consistent with previous processes. Afterwards, the electric energy was cut off when the total feeding amount of raw materials was up to 40 t. Meanwhile, the FMF entered the ending stage, and the smelting condition identification program calculated the duration of each state. Next, the molten lump was designated alphabetically and numerically. The cooling process of the lump took approximately one week. Afterwards, the cooled lump was crushed and sorted. Consequently, the yield and purity of the product were tabulated. **Table 5** shows production data with the original process, whereas, the production data with the improved feeding process are illustrated in **Table 6**. The durations of the four different FMF smelting states are shown in **Fig. 10**. It can be observed from **Fig. 9** and **Fig. 10** that the duration of the overheating state can be shortened by the improved feeding process. Consequently, it can be concluded that feeding raw materials in time results in the decrease of energy consumption per ton.

Table 5 Production data of the original process.

Furnace No.	Power consumption (kWh)	Output (t)	Energy consumption per ton (kWh/t)	Crystal with a purity above 98% (%)
A1	43 440	12.88	3 372.7	52.5
A2	43 500	14.34	3 033.5	52.7
A3	41 618	13.72	3 033.4	55.6
A4	40 943	13.50	3 032.8	53.3
A5	43 524	14.35	3 033.0	52.8
Average	42 605	13.76	3 101.1	53.4

Table 6 Production data of the improved feeding process.

Furnace No.	Power consumption (kWh)	Output (t)	Energy consumption per ton (kWh/t)	Crystal with a purity above 98% (%)
B1	39 064	12.98	3 009.6	52.8
B2	39 706	13.25	2 996.7	51.6
B3	41 199	13.87	2 970.4	53.7
B4	40 425	13.90	2 908.3	52.9
B5	41 533	13.84	3 002.4	52.2
Average	40 389	13.57	2 977.5	52.6

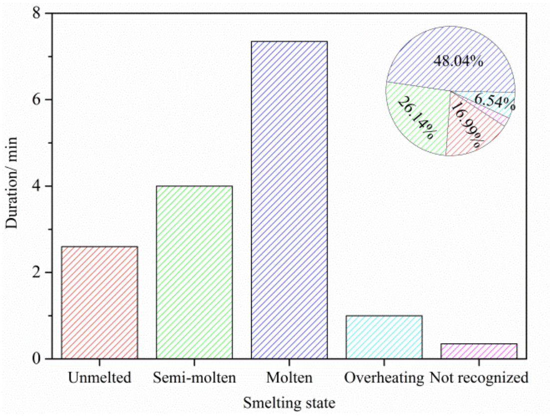

Fig. 10 Duration comparison of the four different FMF smelting states of the improved feeding process.

6.2 Smelting state duration on product purity

During the molten state, the flow velocity of the molten can reach 0.03 m/s. This electromagnetic stirring effect plays a key role in MgO crystallization **(Wang et al., 2014)**. Properly decreasing current injection after entering the molten state could prolong the duration of the molten state. The durations of the four different FMF smelting states of the improved current injection process are shown in **Fig. 11**. **Table 7** shows the production data with the improved feeding process. It can be deduced that decreasing the current injection could increase the duration of the molten state. Consequently, it can be concluded that a long molten state duration results in the increase of the high-purity MgO crystal yield.

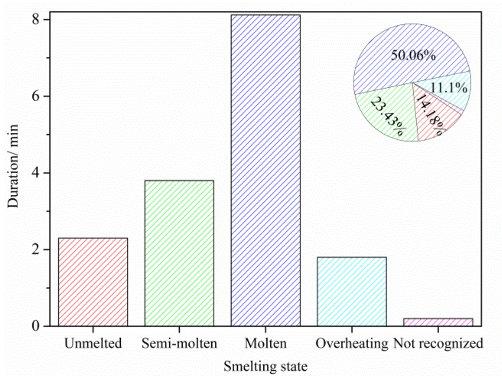

Fig. 11 Duration comparison of the four different FMF smelting states of the improved current injection process.

Table 7 Production data of the improved current injection process.

Furnace No.	Power consumption (kWh)	Output (t)	Energy consumption per ton (kWh/t)	Crystal with a purity above 98% (%)
C1	43 597	13.79	3 161.5	56.2
C2	42 069	13.38	3 144.2	55.7
C3	42 942	13.84	3 102.8	56.1
C4	42 996	13.95	3 082.2	55.8
C5	42 843	13.94	3 073.4	55.6
Average	42 890	13.78	3 122.8	55.9

6.3 Process optimization

A new FMF smelting process based on the acoustic signal was proposed by comprehensively using the two improved processes mentioned above. The detailed smelting process optimizations are as follows:

(1) The smelting condition identification system monitored the smelting state on the status map during each smelting stage.

(2) The identification system judged whether the FMF entered into the molten

state. The current injection decreased as soon as the FMF entered the molten state.

(3) The identification system judged whether the FMF entered the overheating state. Raw materials were added when the FMF entered the overheating state. Thus, the FMF was forced to enter the next unmelted state.

(4) The amount of the raw materials added into the FMF was recorded after each smelting stage.

(5) The shutdown operation was performed when the total amount of raw materials added into the FMF reached 40 t.

Fig. 12 shows the durations of the four different FMF smelting states with the improved process. In addition, the pilot production data of the improved process are shown in **Table 8**. It can be induced that both the energy efficiency and output of high-purity crystal are increased by using the improved smelting process.

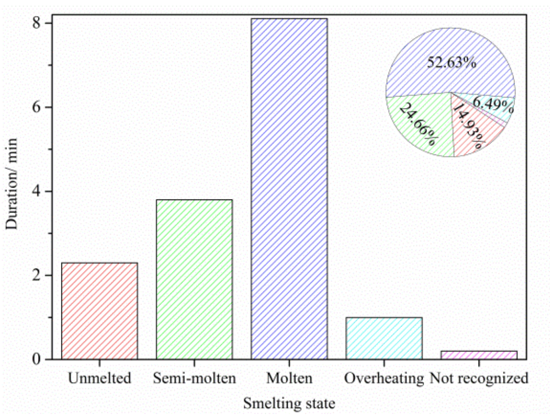

Fig. 12 Duration comparison of the four different FMF smelting states of the improved process.

Table 8 Production data of the improved smelting process.

Furnace No.	Power consumption (kWh)	Output (t)	Energy consumption per ton (kWh/t)	Crystal with a purity above 98% (%)
D1	39 787	13.26	3 000.5	54.9
D2	42 248	14.18	2 979.4	55.3
D3	40 539	13.58	2 985.2	55.0
D4	41 043	13.72	2 991.5	56.0
D5	42 376	14.23	2 977.9	55.8
Average	41 198	13.79	2 986.9	55.4

7 Conclusions

This paper focused on an online fused magnesium furnace smelting condition identification system. The experimental results showed that the system could identify the smelting states with a high accuracy rate. The system was found to be able to improve the energy efficiency during the whole smelting stage. The following conclusions were drawn:

(1) Feeding raw materials as soon as the furnace enters into the overheating stage could effectively reduce the overheating time and reduce the energy consumption per ton during fused magnesia production.

(2) Reducing current injection in the molten stage can prolong the smelting time and promote the purity of MgO crystals.

Acknowledgements

This work was financially supported by the International Science and Technology Cooperation Program of China (2014DFR50880), the Fundamental Research Funds for the Central Universities (DUT16QY35), and the Natural Science Foundation of Liaoning Province (201602173).

References

Bi, S., Han, Y., Lan, H., Liu, L., 2011. Feature selection of arc sound in MIG welding based on core principal component analysis (in Chinese). J. Harb. Univ. Sci. Technol., 16(5), 30–33.

Drouet, M. G., Nadeau, F., 1982. Acoustic measurement of the arc voltage applicable to arc welding and arc furnaces. J. Phys. E: Sci. Instrum., 15, 268–269.

Fu, Y., Wang, N., Wang, Z., Zhang, X., 2015. Running state analysis of electric arc furnace smelting magnesium oxide based on noise signal (in Chinese). Trans. Chin. Electrotechn. Soc., 30(5), 15–22.

Matschullat, T., Rieger, D., Dittmer, B., 2012. Results of foaming slag and scrap meltdown control SIMELT CSM/FSM based on structure-borne sound in electric arc furnace operation. AIST, Atlanta, 2577-2590.

Mohammed, E. M., Sayed, M. A., Moselhy, A., M., Abdelnaiem, A. A., 2013. LPC and MFCC Performance evaluation with artificial neural network for spoken language identification. Int. J. Signal Process., Image Process. and Recognit. Method, 6(3), 55-66.

Xie, S., Jin, F., Krishnan, S., Sattar, F., 2012. Signal feature extraction by multi-scale PCA and its application to respiratory sound classification. Med. & Biol. Eng. & Comput., 759-768.

Hearing, H., Polthier, K., Schmitz, J., 1979. Noise emission of electric furnace steelworks installations. Stahl und eisen, 99(11), 562–568.

Lv, N., Xu, Y., Zhang, Z., 2013. Audio sensing and modeling of arc dynamic characteristic during pulsed Al alloy GTAW process. Sens. Rev. 33(2), 141–156.

Reynolds, Q. G. 2011. The dual–electrode DC arc furnace–modelling insights. J. S. Afr. Inst. Min. Metall., 111(10), 697–704.

Wang, Z., Fu, Y., Wang, N., Feng, L., 2014. 3D numerical simulation of electrical arc furnaces for the MgO production. J. Mater. Process. Technol. 214(11), 2284–2291.

Wu, Y., Zhang, L., Yue, H., Chai, T., 2008. Intelligent optimal control based on

CBR for fused magnesia production (in Chinese). J. Chem. Ind. Eng. (China), 59(7), 1686–1690.

Wu, Y., Zhou, P., Shang, P., Chai, T., 2012. Intelligent operation control for the fused magnesia production. Adv. Mater. Res., 1450–1454.

Wu, Z., Wu, Y., Chai, T., 2011. Intelligent control of fused magnesium furnaces based on SPSA (in Chinese). J. Shanh. Jiaot. Univ., 45(8), 1095–1100

Wu, Z., Wu, Y., Chai, T., Sun, J. 2015. Data–driven abnormal condition identification and self–healing control system for fused magnesium furnace. IEEE Trans. Ind. Electro., 62(3), 1703–1715.

Wu, Z., Wu, Y., Chai, T., Zhang, L., 2009. Intelligent control system of fused magnesia production via rule–based reasoning (in Chinese). J. North. Univ. (Natural Science), 30(11), 1526–1529.

Zweben, S., Karasik, M., 2002. Laboratory experiments on arc deflection and instability. Ir. Steel., 28(2), 75–86.

Table and Figure captions

Table 1 Dimensions of the fused magnesium furnace.

Table 2 Average LPC parameters in diffenrent smelting states.

Table 3 The accumulative contribution rate of each eigenvalue.

Table 4 The principal components of different smelting states.

Table 5 Production data of the original process.

Table 6 Production data of the improved feeding process.

Table 7 Production data of the improved current injection process.

Table 8 Production data of the improved smelting process.

Fig. 1. Schematic diagram of a fused magnesia furnace.

Fig. 2. Experimental setup for the FMF smelting condition identification system.

Fig. 3. The position of the FMF sound measurement point.

Fig. 4. LPC reconstructed waveform of the FMF sound.

Fig. 5 FMF smelting status map.

Fig. 6 LabVIEW block diagram of the FMF smelting condition identification

Fig. 7 LabVIEW front panel of the FMF smelting condition identification program.

Fig. 8 Distribution of the state points on the smelting status map.

Fig. 9 Duration comparison of four different FMF smelting states.

Fig. 10 Duration comparison of the four different FMF smelting states of the improved feeding process.

Fig. 11 Duration comparison of the four different FMF smelting states of the improved current injection process.

Fig. 12 Duration comparison of four different FMF smelting states of improved process.

Table 1 Dimensions of the fused magnesium furnace.

Items	Dimension (mm)
Electrode diameter	350
Diatance between electrodes	880
Electrode operating depth	2 000
Furnace shell diameter	2 500
Furnace shell height	2 000

Table 2 Average LPC parameters in diffenrent smelting states.

State	Unmelted	Semi–molten	Molten	Overheating
a_1	−1.057	−1.317	−1.355	−0.864
a_2	0.398	0.649	1.093	0.371
a_3	−0.391	−0.436	−0.826	−0.368
a_4	0.504	0.345	0.728	0.236
a_5	−0.263	−0.238	−0.366	−0.184
a_6	0.227	0.276	0.610	0.182
a_7	−0.035	0.050	−0.462	−0.049
a_8	0.195	−0.142	0.081	0.077
a_9	−0.218	0.086	−0.061	−0.073
a_{10}	0.071	−0.046	0.111	0.024

Table 3 The accumulative contribution rate of each eigenvalue.

	Eigenvalue	Accumulative contribution rate (%)
λ_1	0.093	78.7
λ_2	0.020	95.8
λ_3	0.005	100
λ_4~λ_{10}	0	100

Table 4 The principal components of different smelting states.

State	b_1	b_2
Unmelted	1.026	−0.125
Semi-molten	1.214	−0.708
Molten	2.092	−0.253
Overheating	0.829	−0.252

Table 5 Production data of the original process.

Furnace No.	Power consumption (kWh)	Output (t)	Energy consumption per ton (kWh/t)	Crystal with a purity above 98% (%)
A1	43 440	12.88	3 372.7	52.5
A2	43 500	14.34	3 033.5	52.7
A3	41 618	13.72	3 033.4	55.6
A4	40 943	13.50	3 032.8	53.3
A5	43 524	14.35	3 033.0	52.8
Average	42 605	13.76	3 101.1	53.4

Table 6 Production data of the improved feeding process.

Furnace No.	Power consumption (kWh)	Output (t)	Energy consumption per ton (kWh/t)	Crystal with a purity above 98% (%)
B1	39 064	12.98	3 009.6	52.8
B2	39 706	13.25	2 996.7	51.6
B3	41 199	13.87	2 970.4	53.7
B4	40 425	13.90	2 908.3	52.9
B5	41 533	13.84	3 002.4	52.2
Average	40 389	13.57	2 977.5	52.6

Table 7 Production data of the improved current injection process.

Furnace No.	Power consumption (kWh)	Output (t)	Energy consumption per ton (kWh/t)	Crystal with a purity above 98% (%)
C1	43 597	13.79	3 161.5	56.2
C2	42 069	13.38	3 144.2	55.7
C3	42 942	13.84	3 102.8	56.1
C4	42 996	13.95	3 082.2	55.8
C5	42 843	13.94	3 073.4	55.6
Average	42 890	13.78	3 122.8	55.9

Table 8 Production data of the improved smelting process.

Furnace No.	Power consumption (kWh)	Output (t)	Energy consumption per ton (kWh/t)	Crystal with a purity above 98% (%)
D1	39 787	13.26	3 000.5	54.9
D2	42 248	14.18	2 979.4	55.3
D3	40 539	13.58	2 985.2	55.0
D4	41 043	13.72	2 991.5	56.0
D5	42 376	14.23	2 977.9	55.8
Average	41 198	13.79	2 986.9	55.4

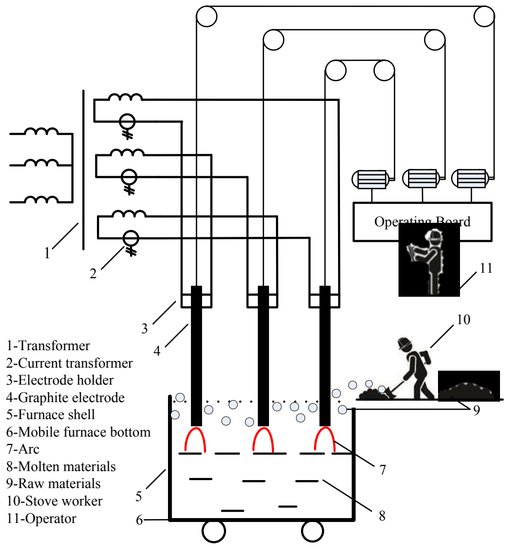

Fig. 1. Schematic diagram of a fused magnesia furnace.

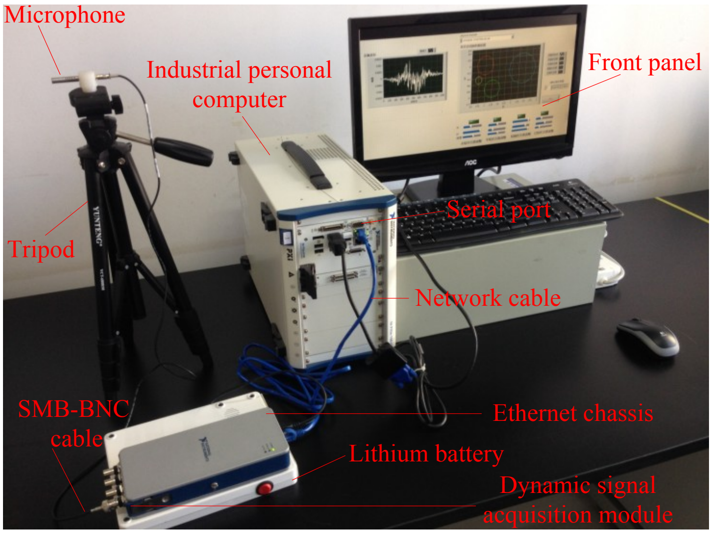

Fig. 2. Experimental setup for the FMF smelting condition identification system.

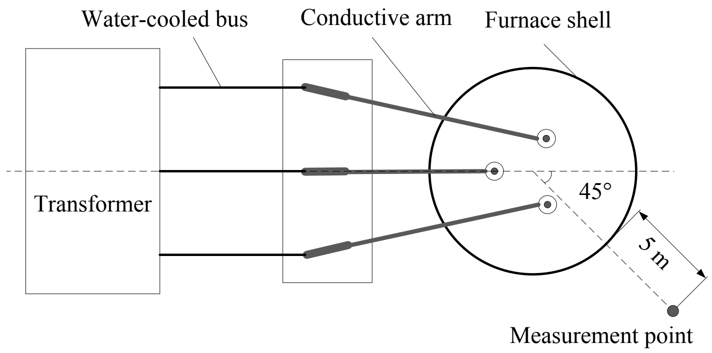

Fig. 3. The position of the FMF sound measurement point.

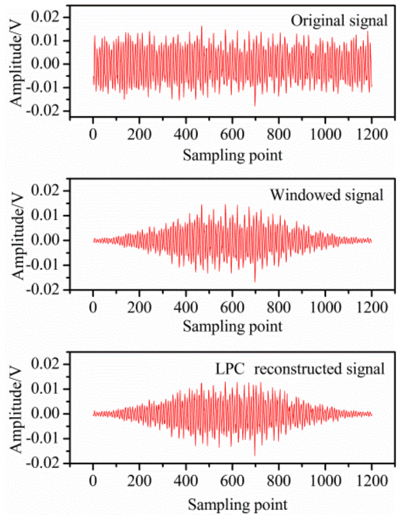

Fig. 4. LPC reconstructed waveform of the FMF sound

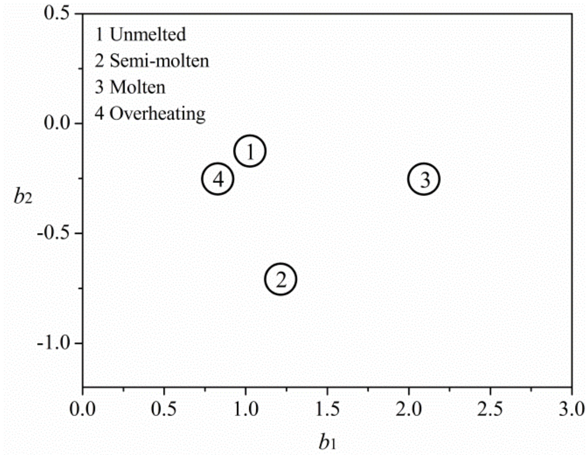

Fig. 5 FMF smelting status map.

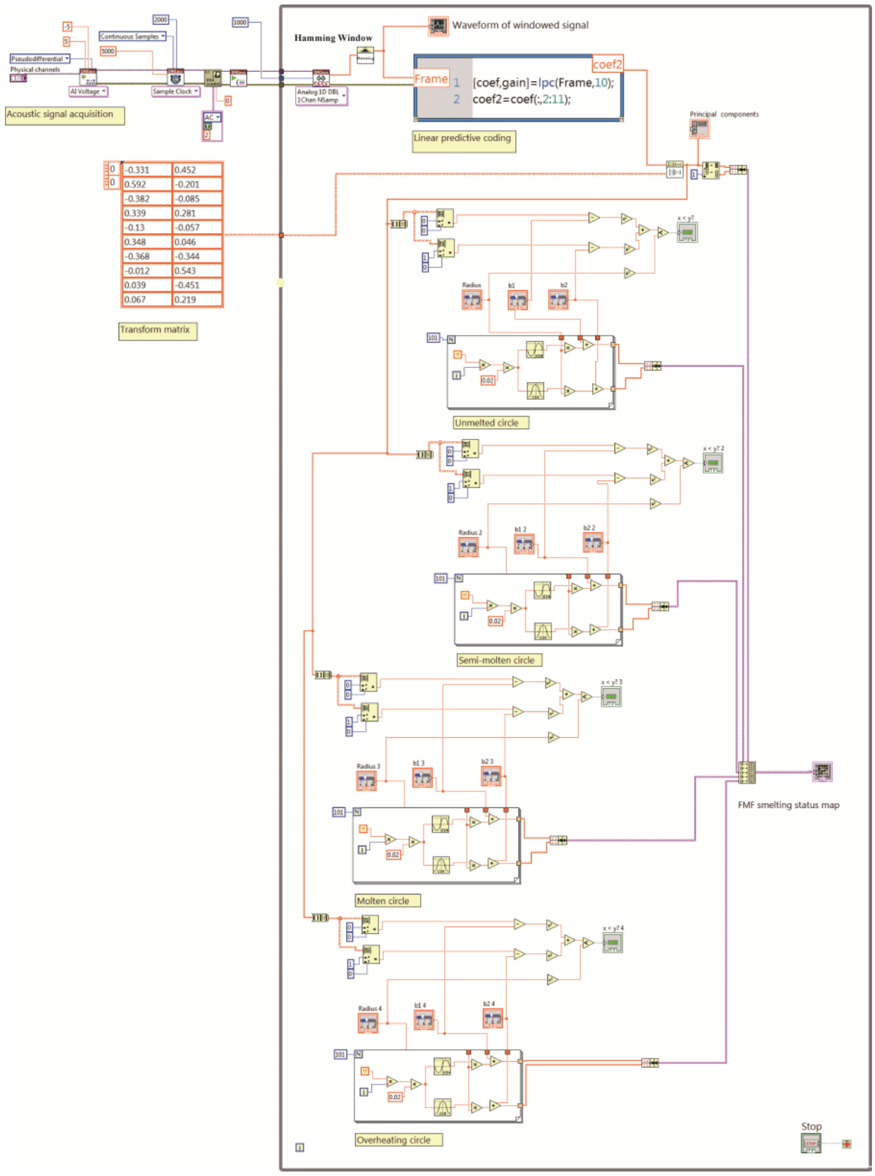

Fig. 6 LabVIEW block diagram of the FMF smelting condition identification program.

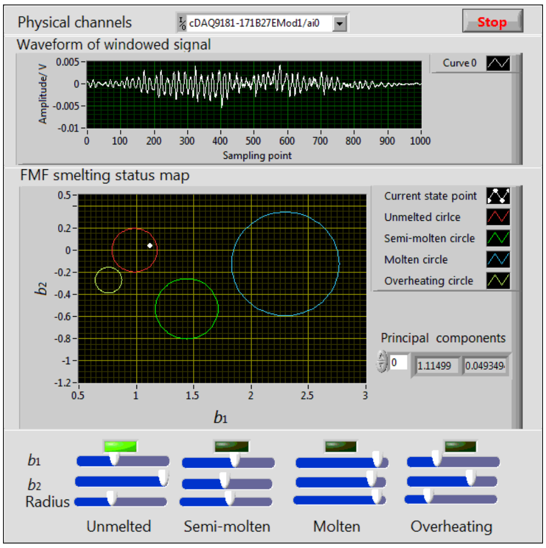

Fig. 7 LabVIEW front panel of the FMF smelting condition identification program.

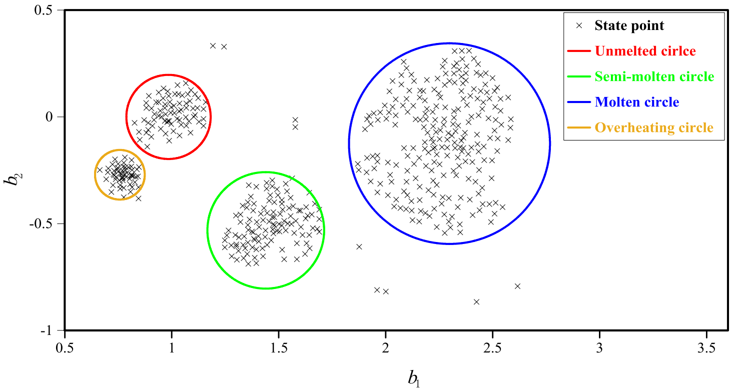

Fig. 8 Distribution of the state points on the smelting status map.

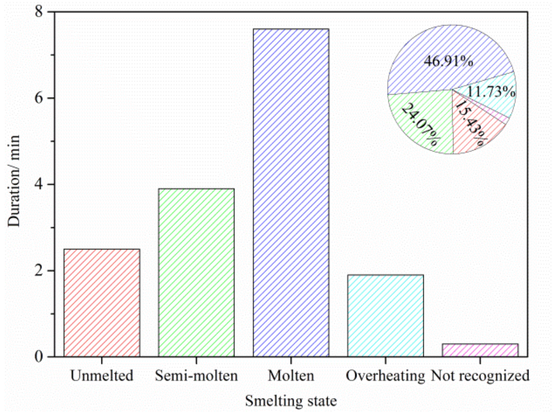

Fig. 9 Duration comparison of the four different FMF smelting states.

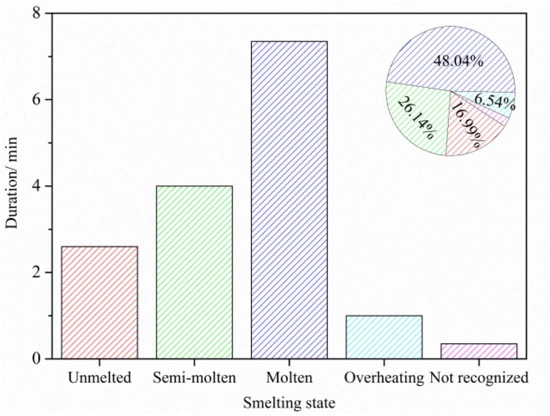

Fig. 10 Duration comparison of the four different FMF smelting states of the improved feeding process.

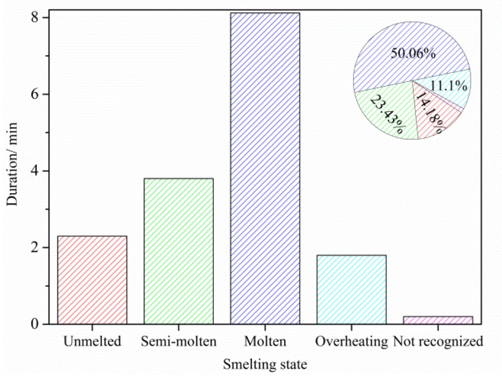

Fig. 11 Duration comparison of the four different FMF smelting states of the improved current injection process.

\

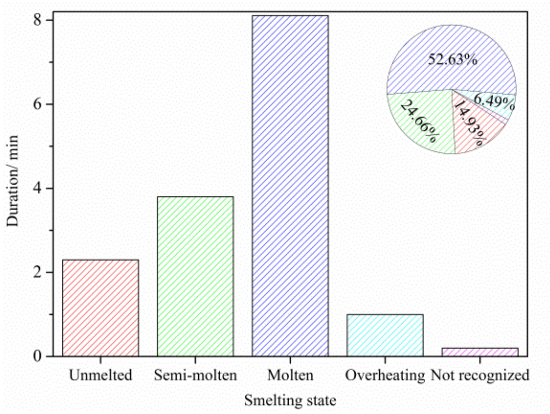

Fig. 12 Duration comparison of the four different FMF smelting states of the improved process.

1